

# PROCEEDINGS OF SPIE

[SPIDigitalLibrary.org/conference-proceedings-of-spie](https://SPIDigitalLibrary.org/conference-proceedings-of-spie)

## High frequency in-core acousto-optic modulation of a suspended core optical fibre

Silva, Ricardo, Webb, David

Ricardo E. Silva, David J. Webb, "High frequency in-core acousto-optic modulation of a suspended core optical fibre," Proc. SPIE 11355, Micro-Structured and Specialty Optical Fibres VI, 113550G (1 April 2020); doi: 10.1117/12.2556801

**SPIE.**

Event: SPIE Photonics Europe, 2020, Online Only, France

# High frequency in-core acousto-optic modulation of a suspended core optical fibre

Ricardo E. Silva\* and David J. Webb

Aston Institute of Photonic Technologies, Aston University, Birmingham, UK, B4 7ET

## ABSTRACT

The confinement of high frequency acoustic waves inside a suspended core fibre (SCF) is numerically investigated for the first time. A 500  $\mu\text{m}$  long acoustic cavity, based on a four-hole SCF, is designed, simulated and evaluated by using the finite element method. The cavity is acoustically excited in the frequency range of 50 - 56 MHz and the induced displacements are integrated along the fibre. A standard single mode fibre is simulated under the same conditions for comparison. The results show strong Lamb acoustic modes oscillating in the silica bridges and overlapping in the SCF core at the resonance of 52.84 MHz. The induced displacement achieves a maximum in the core centre decaying to an almost null value in the cladding. The acoustic wave concentration in the SCF core is 13 times higher compared to the standard fibre, indicating a promising solution to overcome the frequency limitation of the current all-fibre acousto-optic devices. The modulation efficiency is increased without reducing the fibre diameter, making the devices more stable, fast and suitable to modulate all-fibre lasers.

**Keywords:** Lamb acoustic waves, suspended core fibre, acoustic cavity, acousto-optic devices.

## 1. INTRODUCTION

The interaction of fibre Bragg gratings (FBGs) and longitudinal acoustic waves has been successfully employed in tuneable filters, Q-switched and mode-locked fibre lasers<sup>1-4</sup>. In particular, laser output properties, such as, power, wavelength, pulse width and repetition rate are electrically tuned by the frequency and power of the acoustic wave. The acousto-optic modulators are usually composed of a piezoelectric transducer (PZT), an acoustic silica horn and an optical fibre segment axially aligned. The acoustic waves are generated by the PZT and coupled along the fibre with the silica horn. In particular, standard longitudinal acoustic waves are excited along the fibre by fixing the modulator ends. The induced strain  $S_z$  along the fibre core periodically changes the grating period  $\Lambda$  and the modal effective index  $n_{eff}$ , modulating reflection bands beside the Bragg wavelength  $\lambda_B = 2n_{eff}\Lambda$  at twice the acoustic frequency. The reflectivity  $\eta$  and separation  $\Delta\lambda$  of the  $n^{\text{th}}$  order reflection band is given as<sup>5,6</sup>,

$$\eta = \tanh^2 \left[ \frac{\pi \Delta n_{ac} \Gamma}{\lambda_B} L_g J_m \left( \frac{\lambda_a}{\Lambda} S_{z \max} \right) \right], \quad (1)$$

$$S_{z \max} = \sqrt{\frac{2P_{ac}}{YA_s v_{ext}}}, \quad (2)$$

and

$$\Delta\lambda = \frac{f \lambda_B^2}{2n_{eff} v_{ext}}, \quad (3)$$

which depends on the FBG properties (modulation amplitude of the refractive index  $\Delta n_{ac}$ , grating period  $\Lambda$  and length  $L_g$ ), optical fibre properties (modal confinement factor  $\Gamma$ , Young's modulus  $Y$  and fibre cross section  $A_s$ ) and acoustic wave properties (period  $\lambda_a$ , velocity  $v_{ext}$  and acoustic power  $P_{ac}$ ).  $J_n$  is  $n^{\text{th}}$  order the Bessel function of the first kind. In this way, the modulated grating reflectivity  $\eta$  and separation  $\Delta\lambda$  are tuned by the acoustic power  $P_{ac}$  and frequency  $f$ , respectively. Note in (1) and (2) that the acousto-optic efficiency depends on the fibre geometry and material, grating inscription properties and modulator components for acoustic wave generation.

\* r.da-silva@aston.ac.uk; phone 0121 204 5311;

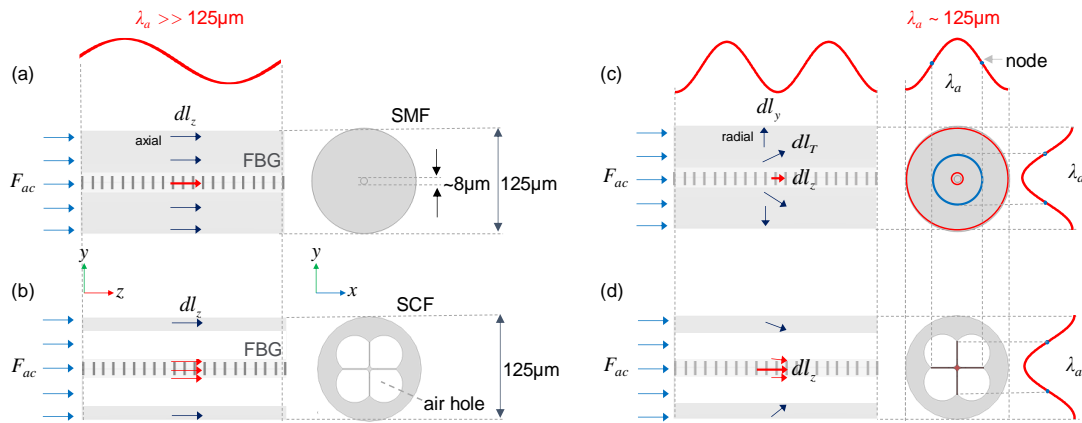


Figure 1. Illustration of the displacements induced by a longitudinal acoustic wave in a (a) SMF and in a (b) SCF for acoustic wavelengths longer than the fibre diameter (a)(b) and of the order of the fibre diameter (c)(d).

Nevertheless, in standard single mode optical fibres (SMFs), the acoustic power is mostly distributed over the fibre cladding, leaving just a small fraction to interact with the optical modes in the core. Fig. 1(a) illustrates a longitudinal acoustic wave along a SMF being excited by a constant sinusoidal acoustic force  $F_{ac}$  at the fibre end. For acoustic frequencies lower than 10 MHz, in which the acoustic wavelength  $\lambda_a$  is considerably longer than the fibre diameter, the acoustic wave induces axial displacements  $dl_z$  along the fibre uniformly distributed in the fibre cross section<sup>7</sup>. However, a small part of the induced displacements is concentrated in the core to interact with the FBG, due to the large ratio between the core and fibre diameters ( $\sim 8/125\mu\text{m}$ ). In addition, the acousto-optic interaction in the core is reduced for acoustic wavelengths comparable to or smaller than the fibre diameter at frequencies higher than 10 MHz<sup>7</sup> (Fig. 1(c)). The fibre cross section works as an acoustic cavity reflecting the acoustic modes radially from the fibre surface to the central axis because the circular geometry. The interference between the maxima and minima (nodes) of the acoustic modes is seen as a radial pattern, as illustrated in Fig. 1(c). Since the fibre length still supports longer wavelengths, the axially induced displacements  $dl_z$  are gradually replaced by radial displacements  $dl_r$  from the core centre to the fibre surface, resulting in a complex overlapped field  $dl_T$  along the fibre<sup>7,8</sup>.

The reduction of the fibre cross section  $A_s$  employing cladding-etched and tapered techniques are useful to strengthen the acousto-optic interaction<sup>1,5</sup>. However, they usually make the device mechanically fragile, additionally exposing the optical properties to be affected by surface contamination. Instead, suspended-core fibres (SCFs) are an emerging option to strengthen the acousto-optic interaction in silica fibres without reducing the fibre diameter<sup>9-11</sup>. The large air holes in the SCF reduce the silica content in the fibre cross section increasing the overlapping between the acoustic and optical power in the core (Fig. 1(b)). For acoustic wavelengths compared to the SCF diameter, the silica bridges work as an acoustic filter for periods  $\lambda_a$  resonating with the bridge length ( $L_b \sim \lambda_a/2$ ), allowing axial acoustic modes to oscillate along the fibre by the silica bridges and core, as illustrated in Fig. 1(d).

In this paper, we have numerically investigated the resonant conditions for the confinement of acoustic waves inside a suspended core fibre at frequencies higher than 50 MHz. A 3D micrometre acoustic cavity based on a real SCF geometry is simulated by using the finite element method. A SMF is also evaluated for comparison and study of the current fibre limitations. A methodology to analyse the induced displacements in the  $xyz$  fibre planes is proposed.

## 2. 3D NUMERICAL MODELLING

Fig. 2 summarizes the numerical modelling and post-processing method employed to assess the acoustically induced displacements in the SCF and SMF. Fig. 2(a) shows the modelled cross sections for both fibres indicating the main dimensions in the  $xyz$  planes. The SCF geometry is based on a pure silica fibre previously employed in an acousto-optic modulator<sup>11</sup>. The fibre is composed of four air holes with diameter of  $\sim 45\mu\text{m}$ . The silica bridges are  $\sim 700\text{nm}$  in thickness forming a silica core with a diameter of  $\sim 5\mu\text{m}$ . The standard single mode optical fibre (SMF-28) has a core diameter of  $8.2\mu\text{m}$ . Both fibres are  $125\mu\text{m}$  in diameter and  $500\mu\text{m}$  in length. A sinusoidal acoustic force with amplitude  $F_{ac} = 3 \times 10^{-3}\text{N}$  is axially applied at one end of the fibre cross section from  $f = 50$  to  $56\text{MHz}$ , in steps of  $20\text{kHz}$ . The other fibre end is fixed (Fig. 2(b)).

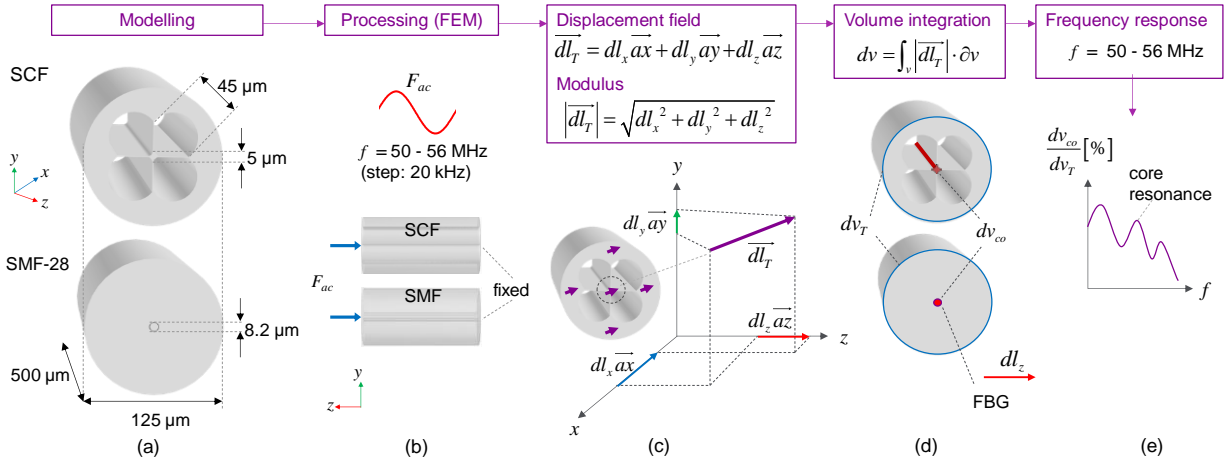


Figure 2. Methodology for modelling the (a) SCF/SMF geometries and (b) the acoustic wave response by using the 3D finite element method (FEM). The induced (c) displacement modulus is (d) integrated along the fibres to determine the (e) resonant frequencies with the highest acoustic power in the fibre core for the considered frequency range.

The acoustically induced displacements are calculated by employing the finite element method (FEM) (commercial package COMSOL Multiphysics 5.4) and the methodology described in Ref.<sup>12</sup>. The following parameters are considered for the silica material in the Mechanics Module: Young's modulus  $Y = 72.5$  GPa, Poisson ratio  $\nu = 0.17$  and density  $\rho = 2200$  kg/m<sup>3</sup><sup>7,13</sup>. The simulations are computed by using a High-Performance Cluster (HPC) providing 71 compute nodes totaling 2000 processor cores and ~9TB memory. The displacement modulus  $|d\vec{l}_T|$  and its  $xyz$  components are evaluated in the SCF cross section, as illustrated in Fig. 2(c). The displacements are integrated along the fibre core ( $dv_{co}$ ) and along the whole fibre ( $dv_T$ ) for both SCF and SMF (Fig. 2(d)). The acoustic modes with the highest power concentration in the core are therefore determined for the considered frequency range (Fig. 2(e)). The displacement profile and wavelength of the resonances are further analysed in detail to identify the resonant conditions for the SCF.

### 3. RESULTS AND DISCUSSION

Fig. 3 shows the frequency response for the SMF for the longitudinal acoustic excitation in the frequency range of  $f = 50 - 56$  MHz. The acoustic modes in detail illustrate the variation of the displacement distribution over the fibre cross section and length with increasing frequency,  $f$ . The analysis of the displacement modulus  $|d\vec{l}_T|$  allows the identification of the nodes (dark blue colour) and the maximum amplitude (dark red colour) of the acoustic wave, providing an indirect measure of the acoustic power distributed in the cladding and fibre core. For the three first modes, the displacements over the fibre surface show an almost periodic profile along the fibre length. However, the reduction of the acoustic period to the order of the fibre diameter, induces radial acoustic waves in the fibre cross section, decreasing the power in the core. This effect becomes evident with increasing frequency from  $f \sim 53$  MHz. The circular fibre geometry works as an acoustic cavity reflecting radially the wave from the core centre to the fibre surface. Consequently, the uniformly distributed axial displacements illustrated in Fig. 1(a) are gradually replaced over the fibre cross section by a superposition of axial and radial displacements along the SMF. It results in a complex modal pattern, as seen e.g., for the acoustic mode at  $f = 55$  MHz. The simulations agree well with the theoretical predictions developed for optical fibres<sup>7</sup>. It is expected that the radial acoustic waves will propagate as surface acoustic waves for acoustic periods significantly shorter than the fibre diameter, since the fibre surface is the unique free boundary for acoustic oscillation. The ratio between core and fibre displacements,  $dv_{co}/dv_T$ , shows peaks in the frequency response indicating the presence of resonances (e.g. the acoustic mode at  $f = 53.68$  MHz). However, a maximum of ~1% of the acoustic wave is concentrated in the fibre core for the considered frequency range.

Fig. 4 shows the frequency response for the SCF. For frequencies up to  $f = 52$  MHz, the induced displacements are mostly concentrated in the cladding, as noted for the SMF. The displacements are oscillating from the core centre to the fibre surface, but no radial profile is observed. The air holes and silica bridges impose a strong acoustic filtering in the fibre cross section, shifting the acoustic power gradually from the cladding to the core with increasing frequency.

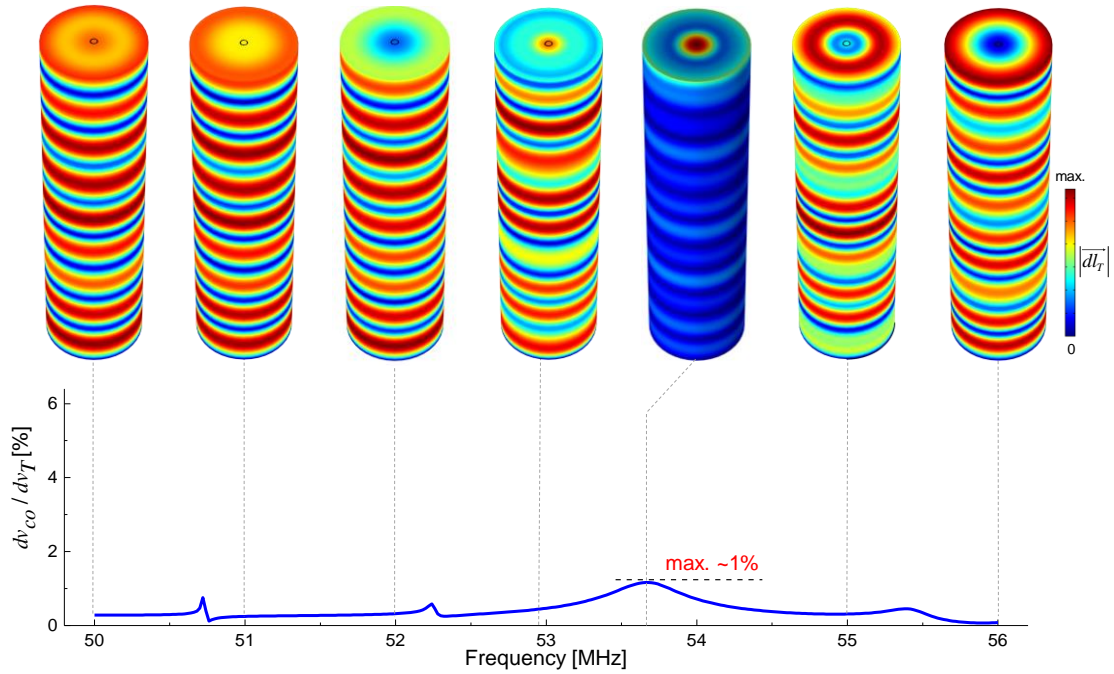


Figure 3. Frequency response for the standard single mode fibre (SMF) under longitudinal acoustic excitation in the frequency range of  $f = 50 - 56$  MHz. The upper detail shows the displacement distribution of seven acoustic modes.

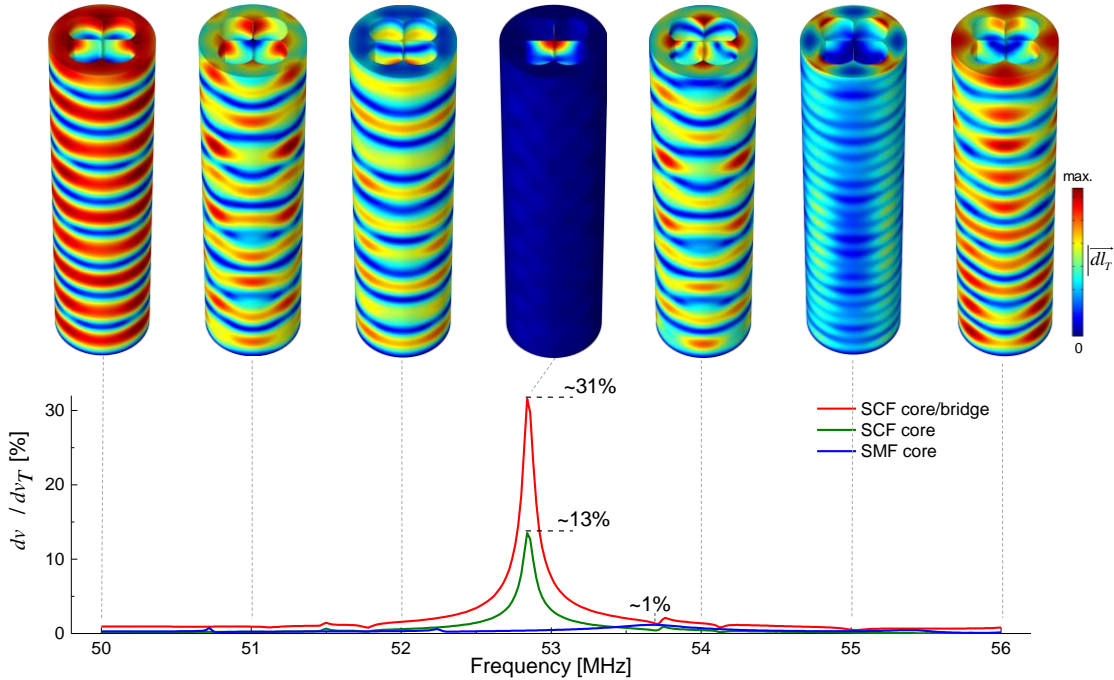


Figure 4. Frequency response for the suspended core fibre (SCF) under longitudinal acoustic excitation in the frequency range of  $f = 50 - 56$  MHz. The upper detail shows the displacement distribution of seven acoustic modes.

At  $f_R = 52.84$  MHz, the acoustic wave is resonant with the fibre diameter and the silica bridges achieving a maximum amplitude at the core centre. The total acoustic power in the silica bridges and fibre core ( $\sim 31\%$ ) indicates a strong confinement of the acoustic wave inside the SCF. The SCF core concentration ( $\sim 13\%$ ) is distinctly higher compared to the SMF ( $\sim 1\%$ ). The 3-dB frequency bandwidth for the SCF resonance is  $\sim 120$  kHz. For frequencies higher than the resonance, the induced displacements gradually leak from the core/bridges to the cladding again.

Fig. 5 shows the displacements in the SCF for the  $yz$  and  $xy$  fibre planes at the resonance of  $f_R = 52.84$  MHz. The simulations reveal a strong Lamb acoustic mode<sup>14</sup> oscillating symmetrically in the fibre cross section from the core centre to bridge ends (Fig. 5(a)). The acoustic waves overlap inducing a maximum displacement in the core centre due to the symmetric disposition of the bridges in the  $xy$  fibre plane. Fig. 5(b) shows the periodic axial displacement  $dl_z$  in the core centre (red curve) with amplitude significantly higher compared to the SMF (blue curve). The acoustic period is  $\lambda_a \sim 118$   $\mu\text{m}$ . Fig. 5(c) shows the displacement distribution in the SCF cross section (along the vertical red dashed line in Fig. 5(a)).  $|dl_T|$  is decomposed into the components  $dl_x$ ,  $dl_y$ , and  $dl_z$ . Note that  $\lambda_a$  is approximately the fibre diameter. The acoustic wave nodes are resonant with the effective total bridge length ( $L_b \sim \lambda_a/2$ ). Consequently, tuning of the resonant frequency  $f_R$  is expected by changing the bridge length  $L_b$  and the core diameter. The displacement in the fibre is almost axial  $dl_z$ , decaying from a maximum in the core centre to an almost null value in the cladding. Moreover, 50% of the acoustic power is concentrated around 40  $\mu\text{m}$  from the core centre, as illustrated in Fig. 5(c).

The strain peak is calculated along the SCF ( $S_z \sim 1.2 \times 10^{-3}$ ) and SMF ( $S_z \sim 2.3 \times 10^{-6}$ ) by employing the proposed method. FBG modulation reflectivity is further estimated with Eq. (1) for both fibres at  $f_R = 52.84$  MHz. An arbitrary grating with modulation amplitude of the refractive index of  $\Delta n_{ac} = 1 \times 10^{-3}$  is considered (parameters detailed in Ref.<sup>9</sup>). The resulting reflectivities  $\eta_{SMF} = 6.72 \times 10^{-6} \%$  (SMF) and  $\eta_{SCF} = 1.67 \%$  (SCF) indicate a SCF modulation efficiency of  $\sim 25 \times 10^4$  higher compared to the SMF.

The simulations confirm the theoretical studies and show intuitively the frequency induced acoustic dispersion in standard fibres, which currently limits the operation of all-fibre acousto-optic devices at frequencies higher than  $f = 10$  MHz. The experimental setup of the proposed device might require the simulation of the real SCFs geometry/material considering defects, imperfections or dimension changes along the fibre, which could shift the resonances and reduce the effective acoustic power in the core. Overall, the strong confinement of optical/acoustic powers in SCFs indicates a promising solution to modulate fibre lasers with repetition rates higher than 100 MHz (reflectivities higher than  $\eta_{SCF} = 1 \%$  are already useful for laser operation<sup>4</sup>).

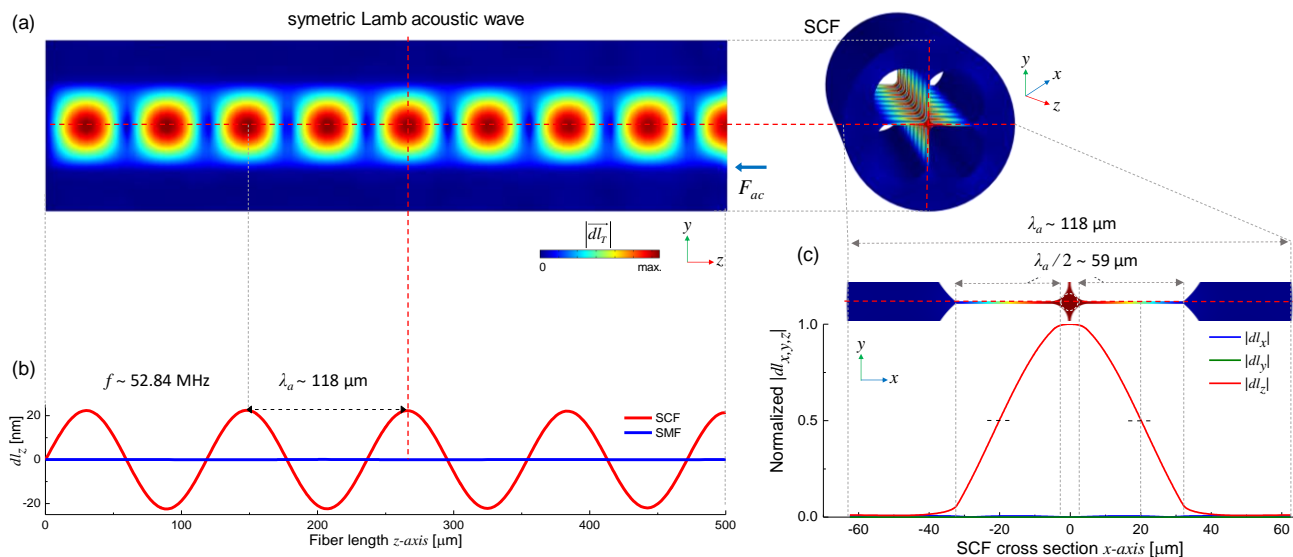


Figure 5. 3D numerical analysis of a symmetric Lamb acoustic wave inside the SCF at the resonance of  $f_R = 52.84$  MHz. The acoustic wave is confined in the (a) silica bridges inducing a (b) periodic displacement/strain at the core centre along the fibre length (dashed red line in Fig. 5(a)). The displacement achieves a (c) maximum in the core centre decaying to an almost null value in the cladding.

## 4. CONCLUSION

In summary, we have proposed and numerically investigated the confinement of Lamb acoustic waves in a suspended core fibre at resonant frequency of  $f_R = 52.84$  MHz. The induced displacements in the SCF core are increased by a factor of 13 compared to the SMF. The acoustic power is mostly distributed in the silica bridges achieving a maximum in the core centre, which is suitable to strengthen the interaction with the optical modes supported by the fibre. The increased modulation efficiency on FBGs recorded in SCF allows the reduction of the modulator size and the acoustic power required to excite the acoustic waves, making the devices more stable and compact for integration with current optoelectronics components. Moreover, the SCF provides better mechanical stability and shielding against external acoustic noise. The results point to a promising solution to mode-lock pulsed fibre lasers with repetition rates higher than 100 MHz.

## ACKNOWLEDGMENT

This project has received funding from the European Union's Horizon 2020 research and innovation programme under the Marie Skłodowska-Curie grant agreement No 713694. We acknowledge the use of Athena at HPC Midlands+, which was funded by the EPSRC on grant EP/P020232/1, in this research, as part of the HPC Midlands+ consortium.

## REFERENCES

- [1] Delgado-Pinar, M., Zalvidea, D., Díez, A., Pérez-Millan, P. and Andrés, M., "Q-switching of an all-fiber laser by acousto-optic modulation of a fiber Bragg grating," *Opt. Express* **14**(3), 1106–1112 (2006).
- [2] Cuadrado-Laborde, C., Díez, A., Cruz, J. L. and Andrés, M. V., "Experimental study of an all-fiber laser actively mode-locked by standing-wave acousto-optic modulation," *Appl. Phys. B* **99**(1–2), 95–99 (2009).
- [3] Villegas, I. L., Cuadrado-Laborde, C., Abreu-Afonso, J., Díez, A., Cruz, J. L., Martínez-Gómez, M. A. and Andrés, M. V., "Mode-locked Yb-doped all-fiber laser based on in-fiber acoustooptic modulation," *Laser Phys. Lett.* **8**(3), 227–231 (2011).
- [4] Silva, R. E., Tiess, T., Becker, M., Eschrich, T., Rothhardt, M., Jäger, M., Pohl, A. A. P. and Bartelt, H., "Acousto-optic modulation of a fiber Bragg grating in suspended core fiber for mode-locked all-fiber lasers," *Laser Phys. Lett.* **12**(4) (2015).
- [5] Liu, W. F., Russell, P. S. J. and Dong, L., "100% efficient narrow-band acoustooptic tunable reflector using fiber Bragg grating," *J. Light. Technol.* **16**(11), 2006–2009 (1998).
- [6] Russell, P. S. J. and Liu, W.-F., "Acousto-optic superlattice modulation in fiber Bragg gratings," *J. Opt. Soc. Am. A* **17**(8), 1421 (2000).
- [7] Engan, H. E., Kim, B. Y., Blake, J. N. and Shaw, H. J., "Propagation and optical interaction of guided acoustic waves in two-mode optical fibers," *J. Light. Technol.* **6**(3), 428–436 (1988).
- [8] Silva, R. E., Tiess, T., Becker, M., Eschrich, T., Rothhardt, M., Jäger, M., Pohl, A. A. P. and Bartelt, H., "All-fiber 10 MHz acousto-optic modulator of a fiber Bragg grating at 1060 nm wavelength," *Opt. Express* **23**(20) (2015).
- [9] Silva, R. E., Hartung, A., Rothhardt, M., Pohl, A. A. P. and Bartelt, H., "Detailed numerical investigation of the interaction of longitudinal acoustic waves with fiber Bragg gratings in suspended-core fibers," *Opt. Commun.* **344**, 43–50 (2015).
- [10] Silva, R. E., Becker, M., Rothhardt, M., Bartelt, H. and Pohl, A. A. P., "Electrically tunable multiwavelength Bragg grating filter acoustically induced in a highly birefringent suspended core fiber," *IEEE Photonics J.* **9**(1) (2017).
- [11] Silva, R. E., Becker, M., Rothhardt, M., Bartelt, H. and Pohl, A. A. P., "Acousto-optic double side-band amplitude modulation of a fiber Bragg grating in a four-holes suspended-core fiber," *J. Light. Technol.* **36**(18), 4146–4152 (2018).
- [12] Silva, R. E., Franco, M. A. R., Neves, P. T., Bartelt, H. and Pohl, A. A. P., "Detailed analysis of the longitudinal acousto-optical resonances in a fiber Bragg modulator," *Opt. Express* **21**(6), 6997–7007 (2013).
- [13] Neves Jr., P. T. and Pohl, A. A. P., "Time analysis of the wavelength shift in fiber Bragg gratings," *J. Light. Technol.* **25**(11), 3580–3588 (2007).
- [14] Vellekoop, M. J., "Acoustic wave sensors and their technology," *Ultrasonics* **36**(1–5), 7–14 (1998).